

Supporting Information

Photo-oxidative Degradation of Methylammonium Lead Iodide

Perovskite: Mechanism and Protection

Yixin Ouyang,^a Yajuan Li,^b Pengchen Zhu,^c Qiang Li,^a Yuan Gao,^c Jianyu Tong,^d Li Shi,^a Qionghua Zhou,^a Chongyi Ling,^a Qian Chen,^a Zhengtao Deng,^d Hairen Tan,^c Weiqiao Deng,^{*b} and Jinlan Wang^{*a}

^aSchool of Physics, Southeast University, Nanjing 211189, China

^bState Key Laboratory of Molecular Reaction Dynamics, Dalian Institute of Chemical Physics, Chinese Academy of Sciences, Dalian 116023, China

^cNational Laboratory of Solid State Microstructures, Collaborative Innovation Centre of Advanced Microstructures, Jiangsu Key Laboratory of Artificial Functional Materials, College of Engineering and Applied Sciences, Nanjing University, Nanjing 210093, China

^dDepartment of Biomedical Engineering, College of Engineering and Applied Sciences, Nanjing National Laboratory of Microstructures, Collaborative Innovation Center of Advanced Microstructures, Nanjing University, Nanjing 210093, China

* Correspondence and requests for materials should be addressed to J.W. (email: jlwang@seu.edu.cn) or to W. D. (email: dengwq@dicp.ac.cn)

Table of Contents

1. Computational models	S1
2. O ₂ , O ₂ ⁻ and H ₂ O adsorption on MAPbI ₃ surfaces.....	S3
3. Stability of oxidized S _{Pb-I} and S _{MA-I}	S8
4. O ₂ adsorption on S _{BA-I} and S _{FPA-I}	S9
5. Hydrophobicity of S _{FPA-I}	S11
6. Adsorption energy summary	S12
7. Supplementary references	S13

1. Computational models

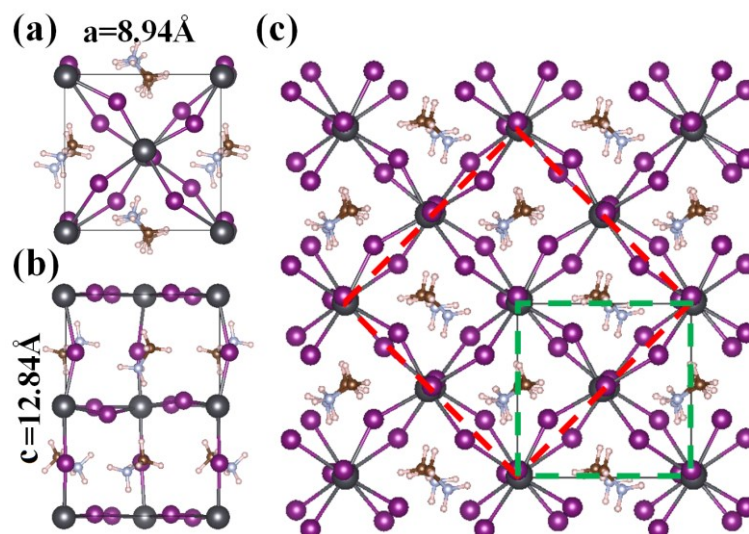


Figure S1. Supercells of bulk tetragonal MAPbI₃. (a) Side and (b) (c) top views of relaxed bulk tetragonal MAPbI₃ structures. The dotted green lines indicate the (1×1) supercell, while the dotted red lines indicate the ($\sqrt{2}\times\sqrt{2}$ R 45°) supercell. The optimized lattice parameters are shown in (a) and (b).

The lattice parameters of bulk tetragonal MAPbI₃ were optimized through a Monkhorst-Pack k-mesh of a 5×5×3 grid and a tetragonal unit cell containing 48 atoms as shown in Fig. S1a and b. The lattice parameters were optimized to be a=b=8.94 and c=12.84 Å, in agreement with previous studies¹⁻³.

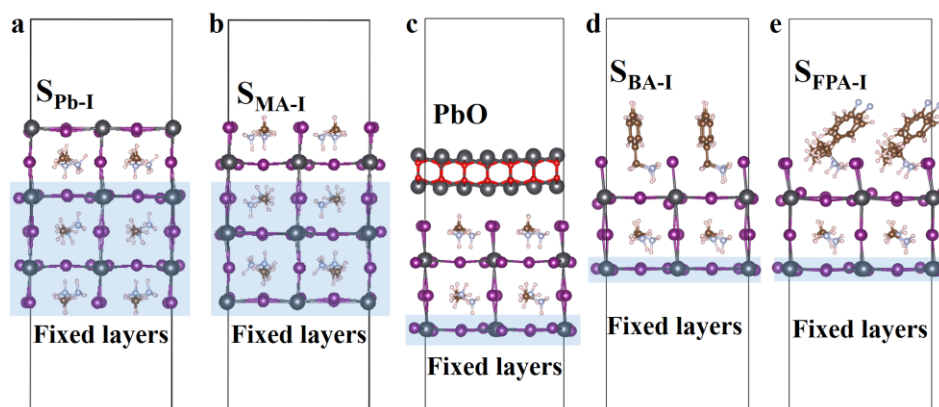


Figure S2. Slab models of different surfaces. Models of PbI_2 -terminated surface, MAI-terminated surface, PbO covered MAI-terminated surface, BAI-terminated surface and FPAI-terminated surface. Inside the blue rectangle regions are fixed while other layers are relaxed.

A periodical slab of two and half layers MAPbI_3 (001) surface was adopted to calculate the adsorption of O_2 , O_2^- , and H_2O on the PbI_2 -terminated surface or the MAI-terminated surface (Fig. S2a and b). To simulate the termination of surface oxidation and the beginning of inner hydration, we employed a periodical slab of one and half layers MAPbI_3 (001) surface covered by PbO (Fig. S2c). In the modeling modified surface, the surface MA molecules were replaced with benzylamine and 2-(4-Fluorophenyl)propan-2-amine (Fig. S2d and e). A vacuum of at least 20 Å in the z-direction was used to avoid the interaction between two periodic units. Oxygen and superoxide were put on the two and half layers (001) surface of MAPbI_3 and the bottom of slabs were fixed to their bulk positions during relaxation, while the rest layers were fully relaxed. The adsorption energies E_{ad} of molecules at different adsorption sites were calculated according to the formula, $E_{\text{ad}} = E_{\text{slab}^+} E_{\text{molecule}} - E_{\text{molecule/slab}}$, where $E_{\text{molecule/slab}}$, E_{slab} , and E_{molecule} are the total energies of the adsorption system, the clean slab model, and the free molecule in vacuum, respectively. An ionic PAW pseudopotential approach^{4,5} is implemented to simulate the molecular anion. The ionic pseudopotential is generated by exciting inner core electrons to the valence shell. To obtain an ionic pseudopotential for a superoxide anion, we use the configuration $1s^{1.5}2s^22p^{4.5}$ in which "half" an electron from 1s shell is put into the valence shell 2p for both the oxygen atoms.

2. O₂, O₂⁻ and H₂O adsorption on MAPbI₃ surfaces

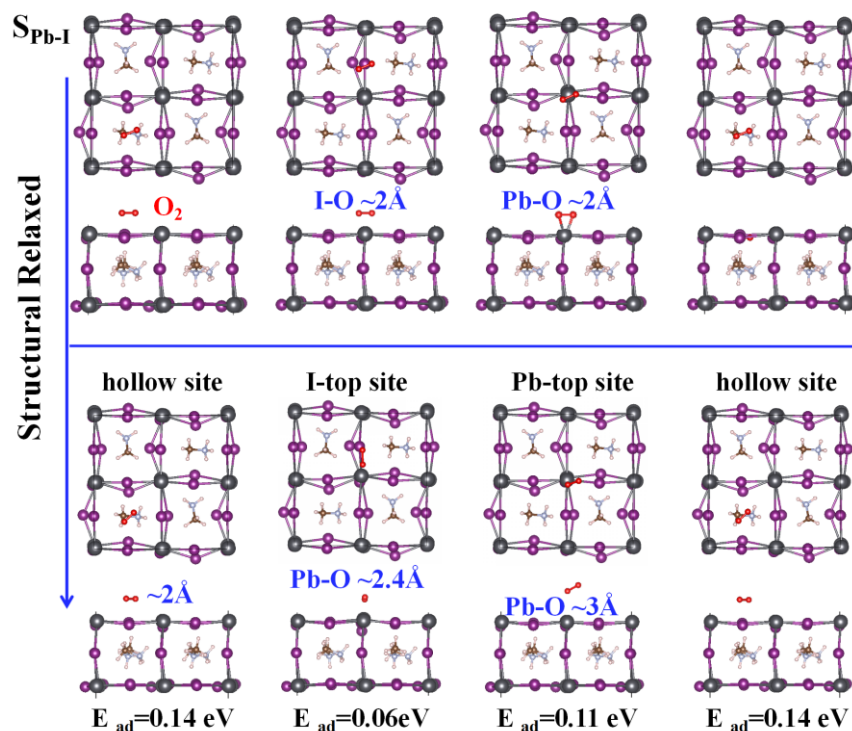


Figure S3. O₂ adsorption on S_{Pb-I}. Structural relaxed of O₂ adsorption on PbI₂-terminated surface. The initial configurations are above the blue line, and the corresponding optimized configurations are under the blue line. The corresponding adsorption energies are also given. Three physisorption sites of O₂ on S_{Pb-I}: hollow site, Pb-top site and I-top site.

In order to get accurate adsorption energy of O₂, zero point energy correction and entropy correction were calculated by:

$$ZPE = \frac{1}{2} \sum_i \hbar \nu_i$$

$$-TS = K_B T \sum_i \ln \left(1 - e^{-\frac{\hbar \nu_i}{K_B T}} \right) - \sum_i \hbar \nu_i \left(\frac{1}{e^{\frac{\hbar \nu_i}{K_B T}} - 1} \right) - K_B T$$

where ν is vibrational frequency and i represent the different modes of vibration for the adsorbates. The amendatory adsorption energy is defined as $E_{ad-cor} = E_{ad} + E_{cor}$, where E_{cor} is the zero point energy correction and entropy correction. The E_{cor} are 0 eV, 0.01 eV and 0.01eV for O₂ adsorption on hollow site, I-top site and Pb-top site, respectively. Obviously, they have negligible impact on the adsorption energy, so it is reasonable to ignore the zero point energy correction and entropy correction.

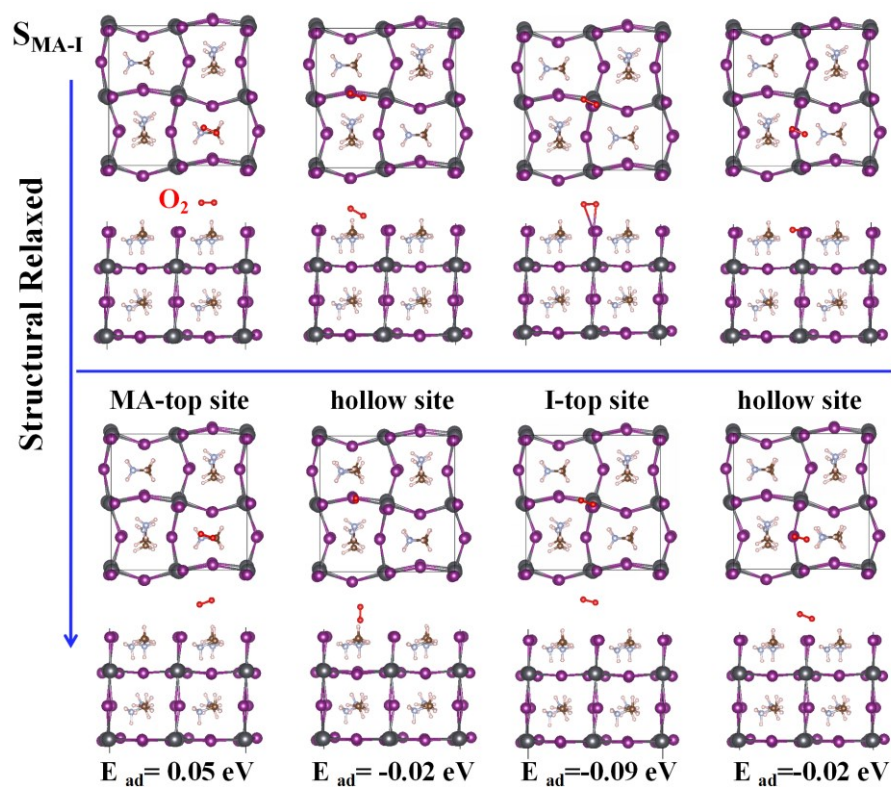


Figure S4. O₂ adsorption on S_{MA-I}. Structural relaxed of O₂ adsorption on MAI-terminated surface. The initial configurations are above the blue line, and the corresponding optimized configurations are under the blue line. The corresponding adsorption energies are also given. Three physisorption sites of O₂ on S_{MA-I} : MA-top site, I-top site and hollow site.

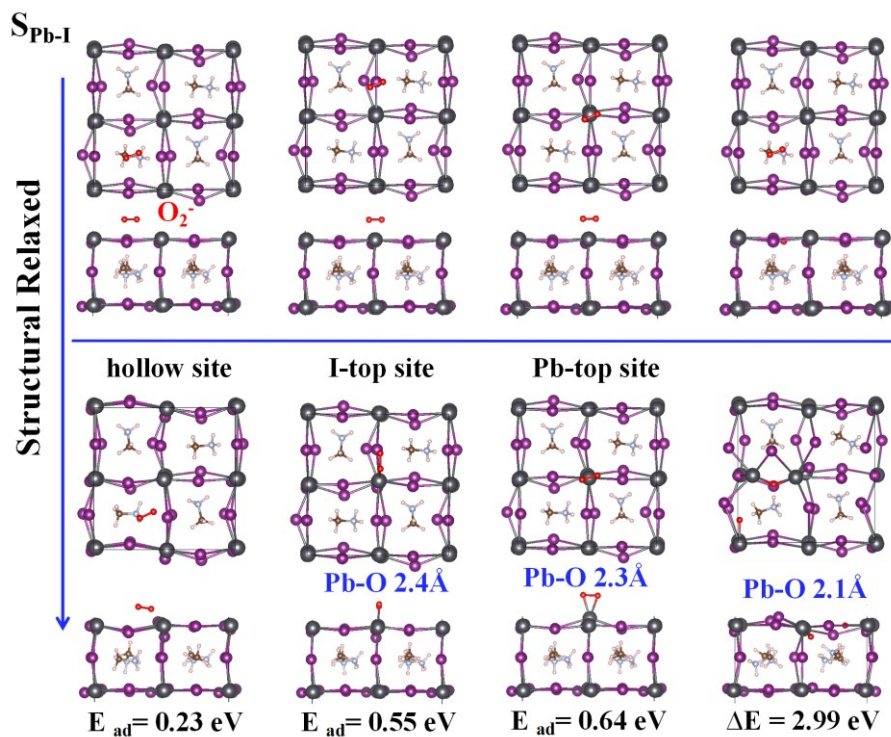


Figure S5. O_2^- adsorption on $\text{S}_{\text{Pb-I}}$. Structural relaxed of O_2^- adsorption on PbI_2 -terminated surface. The initial configurations are above the blue line, and the corresponding optimized configurations are under the blue line. The corresponding adsorption energies are also given. Three physisorption sites of O_2^- on $\text{S}_{\text{Pb-I}}$: hollow site, Pb-top site and I-top site.

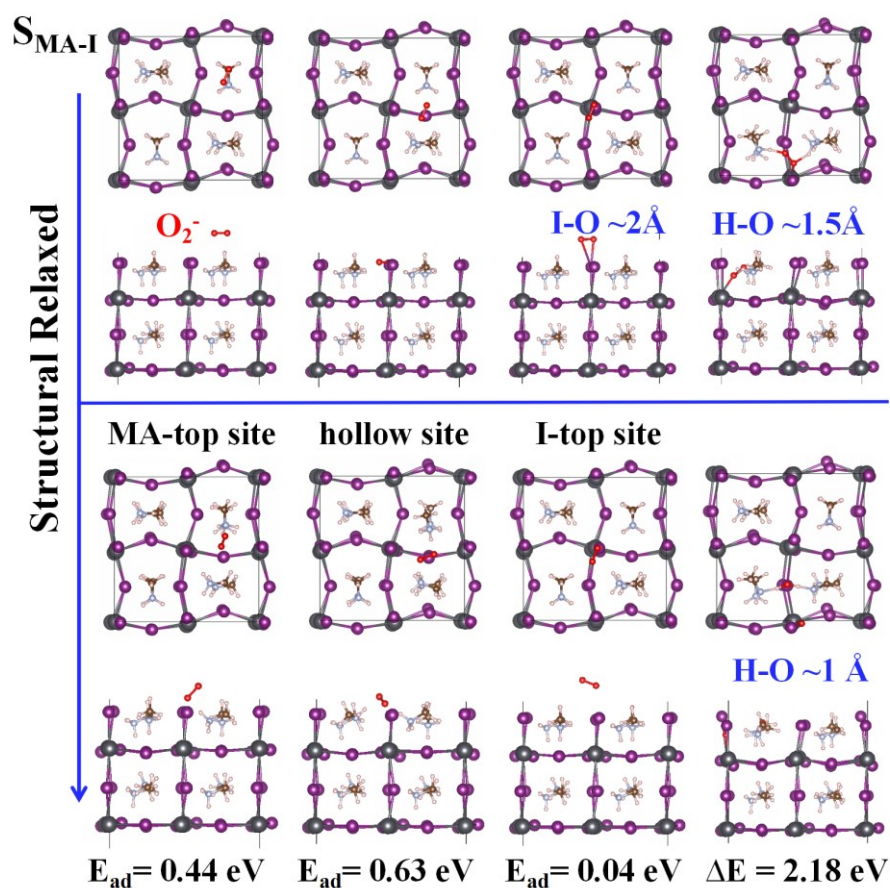


Figure S6. O_2^- adsorption on S_{MA-I} . Structural relaxed of O_2^- adsorption on MAI-terminated surface. The initial configurations are above the blue line, and the corresponding optimized configurations are under the blue line. The corresponding adsorption energies are also given. Three physisorption sites of O_2^- on S_{MA-I} : MA-top site, I-top site and hollow site.

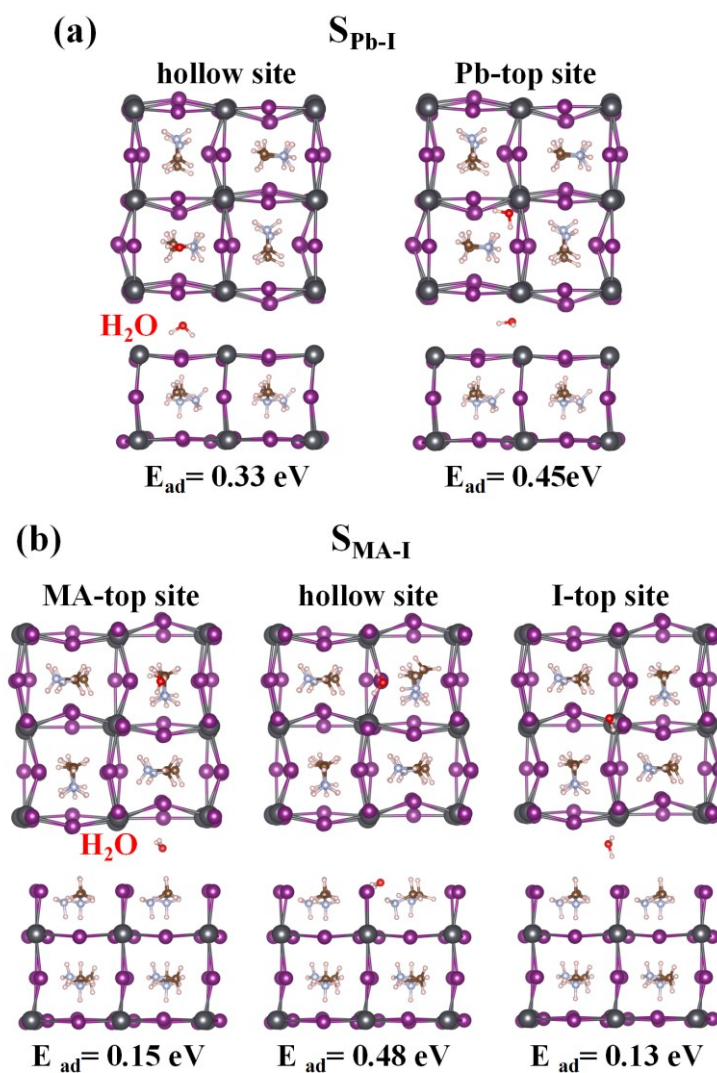


Figure S7. H_2O adsorption on $S_{\text{Pb-I}}$ and $S_{\text{MA-I}}$. Top and side views of the atomic structures of H_2O adsorption on (a) PbI_2 -terminated surface and (b) MAI-terminated surface. The corresponding adsorption energies are also given. Two physisorption sites of H_2O on $S_{\text{Pb-I}}$: hollow site and Pb-top site. Three physisorption sites of H_2O on $S_{\text{MA-I}}$: MA-top site, I-top site and hollow site.

3. Stability of oxidized $S_{\text{Pb-I}}$ and $S_{\text{MA-I}}$

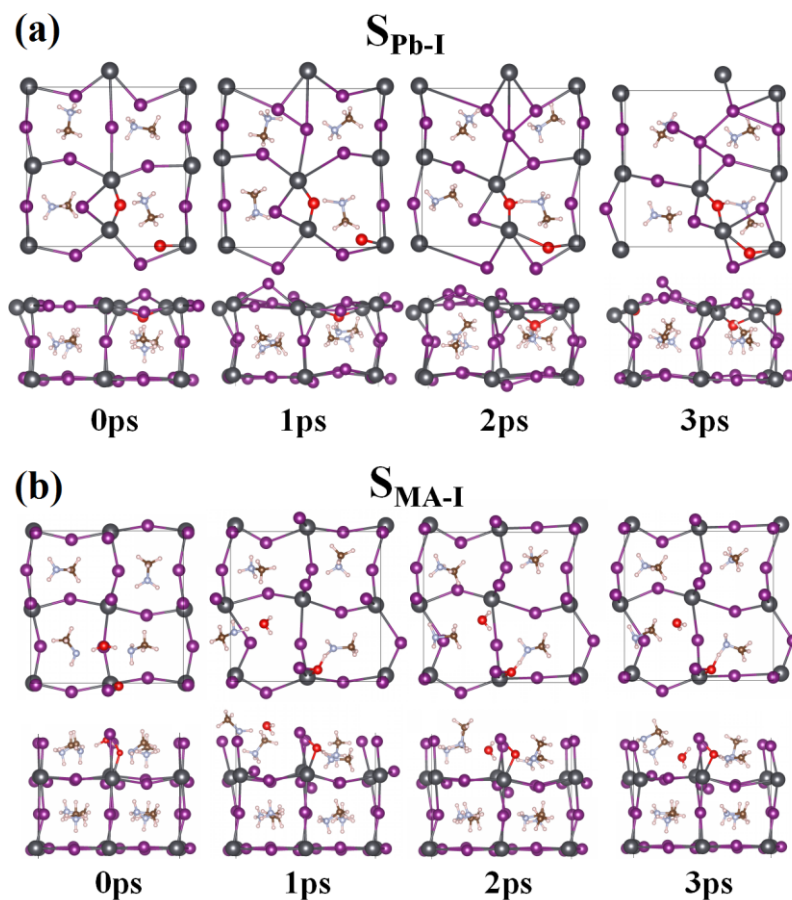


Figure S8. AIMD simulations of oxidized $S_{\text{Pb-I}}$ and $S_{\text{MA-I}}$. Snapshots of AIMD simulations of oxidized (a) PbI_2 -terminated surface and (b) MAI-terminated surface at 300 K.

On the oxidized PbI_2 -terminated surface, Pb atoms and O atoms tend to gather together and form lead oxide. The I atoms in the inorganic frameworks are replaced by the O atoms and tend to form volatile iodine (I_2). On the oxidized MAI-terminated surface, the Pb-O bond results in disintegration of local Pb-I octahedral structure.

4. O₂ adsorption on S_{BA-I} and S_{FPA-I}

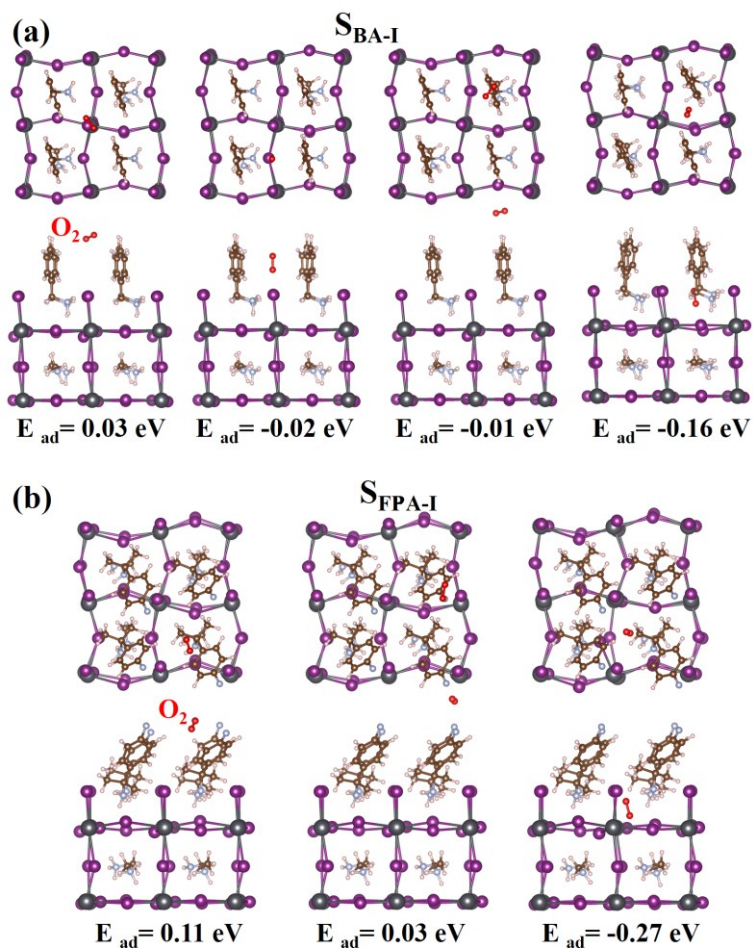


Figure S9. O₂ adsorption on S_{BA-I} and S_{FPA-I}. Top and side views of the atomic structures of O₂ adsorption on (a) BAI-terminated surface and (b) FPAI-terminated surface. The corresponding adsorption energies are also given.

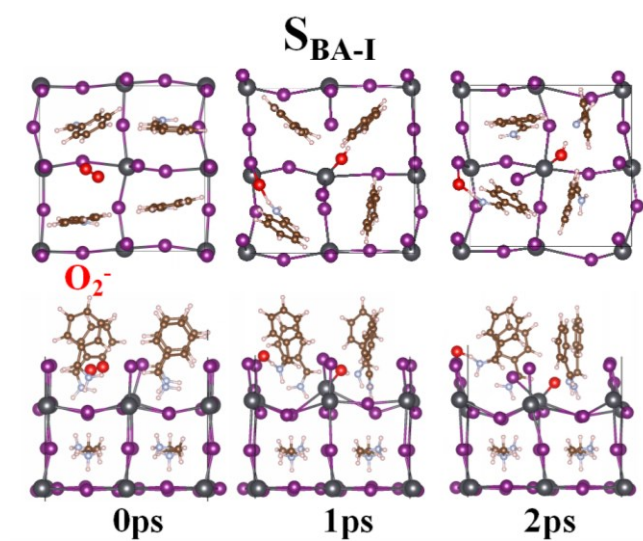


Figure S10. Oxidation of S_{BA-I} . Snapshots of AIMD simulations of O_2^- on BAI-terminated surface at 300 K. The reaction for O_2^- on BA-substituted surface from physisorption to chemisorption quickly occurs at 300 K, and the formation of Pb-O bonds results in disintegration of local Pb-I octahedral structure.

5. Hydrophobicity of $S_{\text{FPA-I}}$

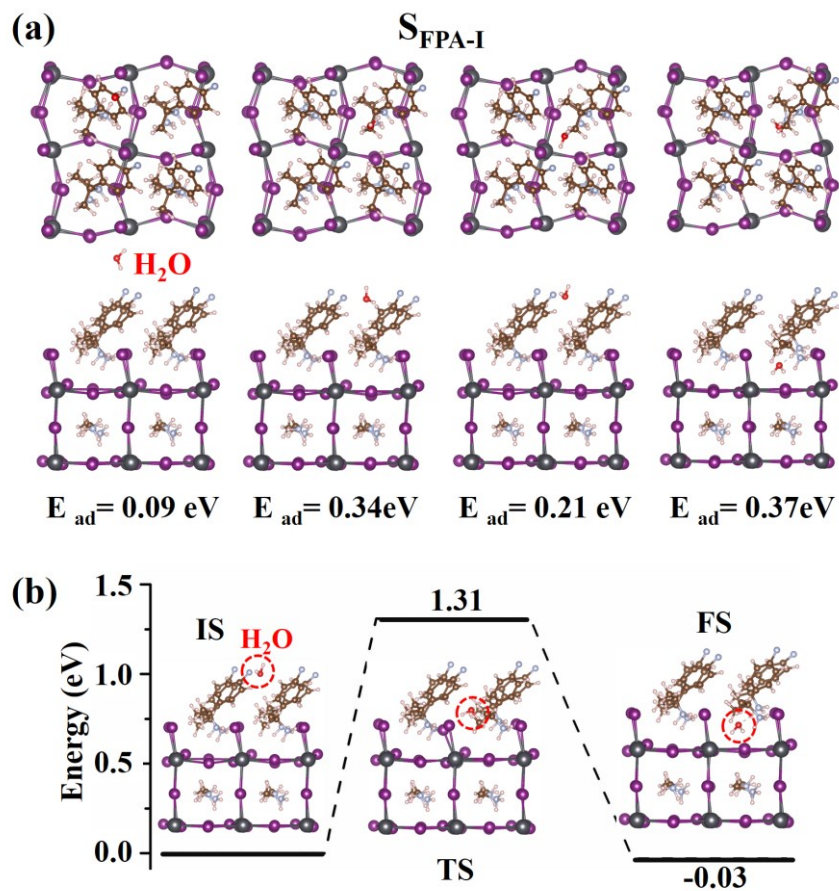


Figure S11. H_2O adsorption and permeation on $S_{\text{FPA-I}}$. (a) Top and side views of the atomic structures of H_2O adsorption on FPAI-terminated surface. The corresponding adsorption energies are also given. (b) The permeation process of H_2O on FPAI-terminated surface.

The adsorption of H_2O on $S_{\text{FPA-I}}$ is weaker than that on $S_{\text{Pb-I}}$ and $S_{\text{MA-I}}$ (Figure S7), and the energy barrier for H_2O diffusing from $S_{\text{FPA-I}}$ to Pb-I frameworks is high. The FPA-substituted surface is completely waterproof.

6. Adsorption energy summary

Table S1. Calculated Adsorption Energies (unit in eV), E_{ad} (eV), of O_2 , O_2^- and H_2O on Surface of $MAPbI_3$

PbI ₂ -terminated surface (S_{Pb-I})			
	hollow	I-top	Pb-top
O_2	0.14	0.06	0.11
O_2^-	0.23	0.55	0.64
H_2O	0.33	to site A	0.45
MAI-terminated surface (S_{MA-I})			
	MA-top	hollow	I-top
O_2	0.05	-0.02	-0.09
O_2^-	0.44	0.63	0.04
H_2O	0.15	0.48	0.13
BAI-terminated surface (S_{BA-I})			
	BA-top	hollow	I-top
O_2	-0.01	-0.02	0.03
FPAI-terminated surface (S_{FPA-I})			
	FPA-top	hollow	I-top
O_2	0.03	to site C	0.11
H_2O	0.09	0.34	0.21

7. Supplementary references

1. C. C. Stoumpos, D. H. Cao, D. J. Clark, J. Young, J. M. Rondinelli, J. I. Jang, T. H. Joseph, G. K. Mercuri, *Chem. Mater.* **2016**, *28*, 2852-2867.
2. W. Hao, X. Chen, S. Li, *J. Phys. Chem. C* **2016**, *120*, 28448-28455.
3. K. P. Ong, T.W. Goh, Q. Xu, A. Huan, *J. Phys. Chem. Lett.* **2015**, *6*, 681-685.
4. L. Kohler, G. Kresse, *Phys. Rev. B* **2004**, *70*, 165405.
5. L. Leung, T. Lim, Z. Ning, J. C. Polanyi, *J. Am. Chem. Soc.* **2012**, *134*, 9320.